IEEJ Journal of Industry Applications
Vol.8 No.4 pp.623–631 DOI: 10.1541/ieejjia.8.623

Paper

Robust 2-DoF Controller Design using H_∞ Synthesis for Flexible Robots

Tran Vu Trung[*a)] Student Member, Makoto Iwasaki[*] Senior Member

(Manuscript received July 20, 2018, revised Jan. 25, 2019)

Fast-response with high-precision positioning for industrial robots is an indispensable requirement in a wide range of applications. Nonetheless, resonant vibrations due to flexibilities in mechanical structures generally deteriorate their motion performance. A practical approach to achieve fast and precise positioning is to use a two-degree-of-freedom (2-DoF) control system with feedback and feedforward compensators. Conventionally, a cascade feedback control system is constructed based on P-PI control, where the position and velocity controllers are respectively implemented using a proportion (P) and a proportion-integrator (PI). The paper proposes robust vibration suppression using H_∞ control as an alternative design for the feedback compensators in the 2-DoF cascade closed-loop control framework of a flexible robot arm. Acceleration feedback is also applied to improve the control performance. The effectiveness of the proposed design has been verified by conducting experiments using a prototype.

Keywords: flexible robots, H_∞ controller design, acceleration feedback, robust control, vibration suppression

1. Introduction

Modern industrial manipulators are usually required to meet the industry's demands for high-speed high-accuracy applications. The requirement of precision gear systems has resulted in an increasing implementation of the strain wave gearing (SWG) in industrial robots thanks to its compactness, high gear ratios, and zero backlash [(1)]. Nevertheless, elastic deformation in the flexspline of SWG often leads to negative effects on control performance. Besides, there has been an increasing interest in the use of soft materials with high flexibility to manufacture robots for safe interaction with humans [(2)]. Consequently, various mechanical resonant vibrations are excited in robot arms with SWG. Robust vibration suppression problem in motion control of flexible robots is then required to deal with many sources of disturbances and uncertainties, such as load variation and nonlinear properties.

H_∞ optimization is widely considered an efficient and powerful tool to synthesize robust controllers. There are two main H_∞ optimization-based approaches to obtain a controller that gives the desired robust performance: *loop-shaping synthesis* and *mixed-sensitivity synthesis*. The H_∞ loop-shaping synthesis using Glover-McFarlane method [(3)] combines shaping of the open-loop transfer function with H_∞ robust stabilization, while the H_∞ mixed-sensitivity synthesis [(4)] and its variations directly shape closed-loop transfer functions [(5)].

In robotics, H_∞ controller designs have been also reported in many publications. Sage et al. conducted a survey of linear H_∞ schemes for robot manipulators described by rigid models in 1999 [(6)]. Recently, H_∞ control is applied to flexible robots in various approaches. Axelsson et al. proposed H_∞ mixed-sensitivity and loop-shaping designs for a flexible joint in 2014 [(7)]. Makarov et al. introduced an application of H_∞ framework to design both feedback and feedforward controllers in 2-DoF control system in 2016 [(8)].

In the above papers, the closed-loop with only position feedback was mentioned. To avoid low-frequency fluctuation due to additional damping, velocity feedback should be added in positioning systems [(9)]. In industrial applications, a velocity control loop is often cascaded with a position loop, which forms the cascade closed-loop control structure [(10)].

On the other hand, the acceleration feedback (AFB) has been successfully applied to improve the control performance of flexible manipulators. Zhang [(11)] conducted a comparison of speed control schemes for two-mass systems, which shows that the system with AFB is better than the one without AFB in the disturbance rejection. Kino et al. [(12)] proposed a multiple AFB design for the flexible robot modeled by a three-mass system, where accelerations at both sides of the robot link were fed back.

This paper presents a novel 2-DoF cascade closed-loop control design with H_∞ synthesis-based feedback controller, together with co-prime factorization-based feedforward compensators [(13)] and acceleration feedback, for the robot arm modeled as a three-mass system. The design concentrates on suppressing the vibrations due to the low stiffnesses of the robot link and the gearing, as well as to ensure robustness against load parameter variations.

2. Conventional Control System of Robot Arm

2.1 Configuration and Modeling of Experimental Setup Figure 1 shows a schematic configuration of experimental setup. The robot arm used in experiments is a horizontal single-axis one. It consists of an AC servo motor, a strain wave gearing, and a flexible link. At both sides of the gearing, optical encoders are installed to enable double feedback control. The encoder mounted on the motor shaft is used to measure the motor position, while the other one on arm side of the gearing is attached to feed back the position

a) Correspondence to: Tran Vu Trung. E-mail: tranvutrung@ieee.org
* Department of Electrical and Mechanical Engineering, Nagoya Institute of Technology
Gokisho, Showa-ku, Nagoya, Aichi 466-8555, Japan

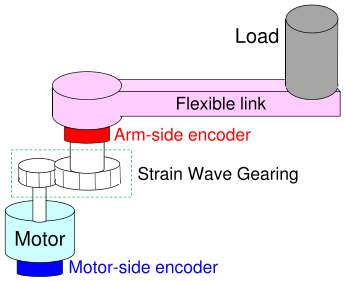

Fig. 1. Configuration of experimental robot arm

Table 1. Specifications of experimental setup

Motor rated torque	1.27 Nm
Motor maximum instant torque	3.8 Nm
Motor rated speed	3000 rpm
Motor-side encoder resolution	2^{17} pulse/rev
Arm-side encoder resolution	2^{20} pulse/rev
Gear ratio	50

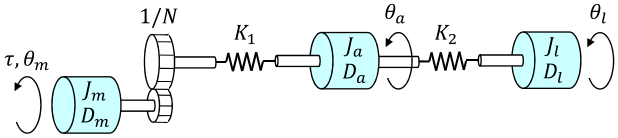

Fig. 2. Schematic diagram of three-mass system

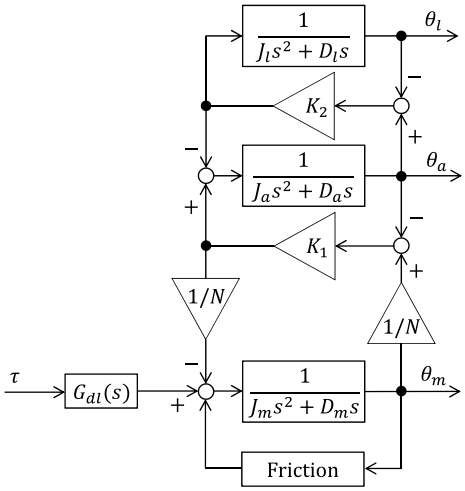

Fig. 3. Block diagram of three-mass flexible model

of gearing's output. In addition, some cylindrical loads are stacked at the arm tip. The total load weight can be switched between 10, 12.5, and 15 kg. Specifications of the experimental setup are listed in Table 1.

Figure 2 shows a simplified schematic diagram of the robot arm as a three-mass system. The movements of the whole system are assumed to be around an axis not affected by gravity [14]. Flexibilities within the gearing and the link are described by two linear springs. The block diagram of the three-mass flexible model is shown in Fig. 3, where τ is the input torque; $G_{dl}(s) = e^{-Ls}$ is the L-second delay component; N is the gear ratio; θ_m, θ_a, and θ_l are the positions of motor, gearing's output, and load at arm tip, respectively; J_m, J_a, and J_l are the moments of inertia; D_m, D_a, and D_l are the viscous damping coefficients; K_1 and K_2 are the gearing and link stiffnesses, respectively; f is the nonlinear friction.

Curve fitting-based identification results are shown in Fig. 4, where blue lines represent experimental sine-sweep data while red lines represent for the three-mass model's characteristics. They all exhibit two vibration modes: the first results from the flexibility of the link, while the second is excited due to the elastic deformation of the gearing. Notice here that the phase characteristics in θ_m and θ_a are different at the two modes: in-phase at the first vibration frequency, while out-of-phase at the second one.

The model parameters for the 15 kg load case, which is chosen to be nominal model, are listed in Table 2. As for the other cases, there exist considerable variations of load parameters, shown in Table 3. In particular, J_l decreases by 22% and 30%, while K_2 increases by 33% and 120%, for 12.5 and 10 kg loads, respectively.

2.2 2-DoF Cascade Closed-loop Control System

The conventional one-degree-of-freedom (1-DoF) cascade closed-loop control system of the robot arm, shown in Fig. 5, includes two cascaded feedback loops: an arm position loop outside and a motor velocity control loop inside. The position controller is a proportion (P), and the velocity controller is a proportion-integrator (PI) compensator:

$$C_p(s) = K_{pp}, \quad \cdots\cdots (1)$$

$$C_v(s) = K_{vp}\left(1 + \frac{1}{T_{vi}s}\right), \quad \cdots\cdots (2)$$

where the controller default parameters of the experimental setup are listed in Table 4.

The conventional two-degree-of-freedom (2-DoF) control framework, on the other hand, is composed of the above feedback (FB) control system and feedforward (FF) compensators. It is acknowledged to be a practical approach [15] for achieving fast-response motion performance. Figure 6 shows a block diagram of the 2-DoF cascade control system, where the FF components are designed by a co-prime factorization.

In detail, assuming that the transfer functions from the input torque to the motor and arm positions are expressed by

$$P_m(s) = \frac{\theta_m(s)}{\tau(s)} = \frac{P_{Nm}(s)}{P_D(s)}, \quad \cdots\cdots (3)$$

$$P_a(s) = \frac{N\theta_a(s)}{\tau(s)} = \frac{P_{Na}(s)}{P_D(s)}, \quad \cdots\cdots (4)$$

the FF compensators can be determined as follows:

$$N_m(s) = \frac{P_{Nm}(s)}{F_c(s)}, \; N_a(s) = \frac{P_{Na}(s)}{F_c(s)}, \; D(s) = \frac{P_D(s)}{F_c(s)}, \quad \cdots\cdots (5)$$

where $F_c(s)^{-1}$ is a low-pass filter with free parameters, which makes the transfer functions of FF compensators to be proper.

The closed-loop transfer function from the reference r to the arm position $N\theta_a$ then becomes:

$$T_{yr}(s) = N_a(s) = \frac{P_{Na}(s)}{F_c(s)}. \quad \cdots\cdots (6)$$

Theoretically, the FF compensators should be computed directly from transfer functions of three-mass model mentioned in section 2.1. In practice, however, the three-mass-model-based FF controllers require a complicated implementation because of their high order and excessive gains. Therefore,

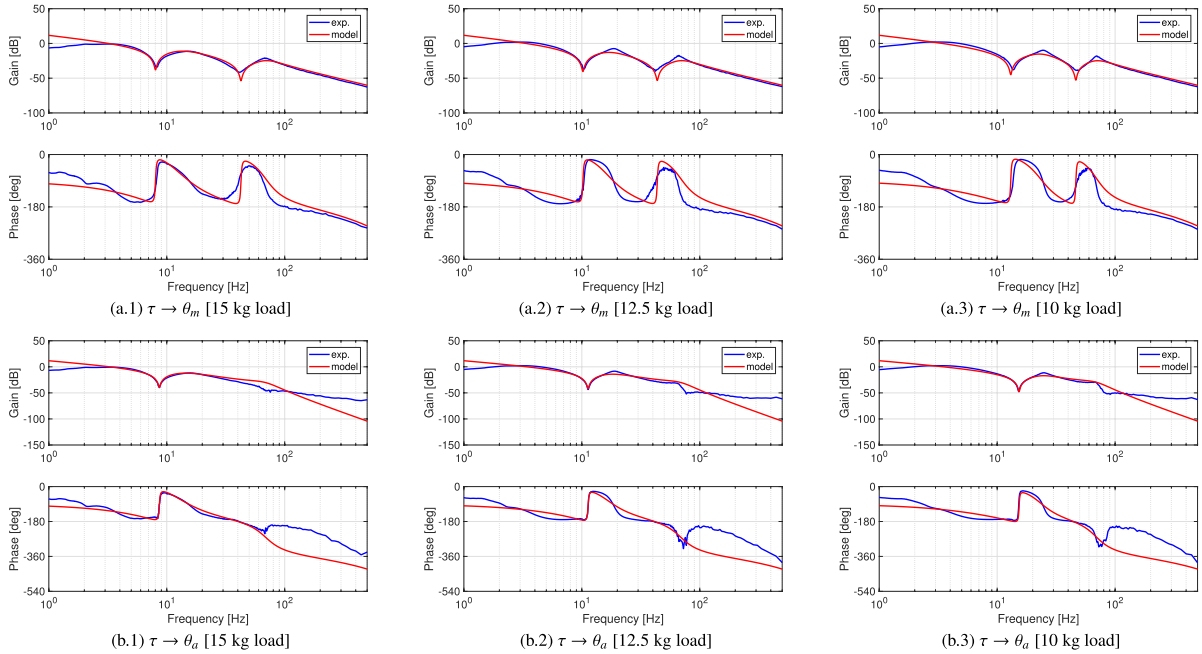

(a.1) $\tau \to \theta_m$ [15 kg load] (a.2) $\tau \to \theta_m$ [12.5 kg load] (a.3) $\tau \to \theta_m$ [10 kg load]

(b.1) $\tau \to \theta_a$ [15 kg load] (b.2) $\tau \to \theta_a$ [12.5 kg load] (b.3) $\tau \to \theta_a$ [10 kg load]

Fig. 4. Bode plots of actual plant and three-mass model for different load weights

Table 2. Parameters of nominal three-mass model

N	50	K_1	40000 Nm/rad	K_2	6200 Nm/rad
J_m	1.04×10^{-4} kgm^2	J_a	0.65 kgm^2	J_l	2.1 kgm^2
D_m	1.4×10^{-4} Nms/rad	D_a	5 Nms/rad	D_l	3 Nms/rad

Table 3. Variations of load parameters

Load weight	J_l	ΔJ_l	K_2	ΔK_2
15 kg	2.1 kgm^2	0%	6200 Nm/rad	0%
12.5 kg	1.64 kgm^2	−22%	8250 Nm/rad	+33%
10 kg	1.47 kgm^2	−30%	13650 Nm/rad	+120%

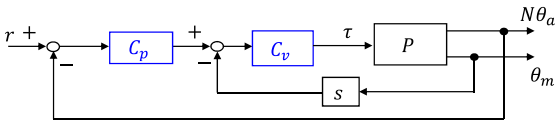

Fig. 5. Block diagram of 1-DoF cascade closed-loop control system

Table 4. Parameters of P-PI controller

K_{pp}	K_{vp}	T_{vi}
25.1327 s^{-1}	0.0391 Nms/rad	0.03 s

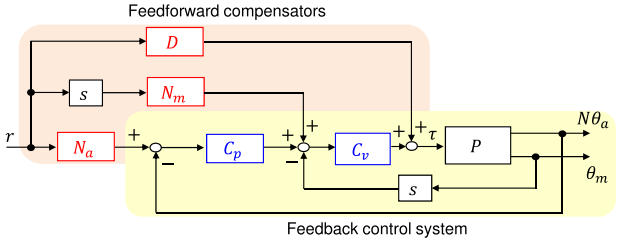

Fig. 6. Block diagram of 2-DoF cascade closed-loop control system

in this design, the FF compensators can be calculated using an approximate two-mass model of the plant, whose block diagram is shown in Fig. 7. In this approximation, the joint

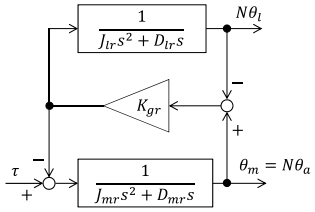

Fig. 7. Block diagram of reduced two-mass model

is assumed to be rigid, the nonlinear friction and phase delay components are also neglected, hence we get:

$$J_{mr} = J_m + \frac{J_a}{N^2}, \quad D_{mr} = D_m + \frac{D_a}{N^2}, \quad \cdots\cdots\cdots\cdots (7)$$

$$J_{lr} = \frac{J_l}{N^2}, \quad D_{lr} = \frac{D_l}{N^2}, \quad K_{gr} = \frac{K_2}{N^2}. \quad \cdots\cdots\cdots\cdots (8)$$

The transfer functions of the plant described by the two-mass model can be easily obtained as follows [16]:

$$P_{Na}(s) = P_{Nm}(s) = J_{lr}s^2 + D_{lr}s + K_{gr}, \quad \cdots\cdots\cdots (9)$$

$$P_d(s) = J_{mr}J_{lr}s^4 + (J_{mr}D_{lr} + J_{lr}D_{mr})s^3 + (D_{mr}D_{lr} + K_{gr}J_{mr} + K_{gr}J_{lr})s^2 + K_{gr}(D_{mr} + D_{lr})s. \quad \cdots\cdots\cdots\cdots (10)$$

The low-pass filter $F_c(s)^{-1}$ should be then the following 4^{th}-order one:

$$F_c(s)^{-1} = K_{gr}^{-1}\left(\frac{\omega_c}{s + \omega_c}\right)^4, \quad \cdots\cdots\cdots\cdots (11)$$

where the cut-off frequency ω_c is chosen such that the control bandwidth is as wide as possible. The factor K_{gr}^{-1} is included to make the closed-loop transfer function $T_{yr}(s)$ in (6) equal to 1 at $s = 0$, then to eliminate position error at steady state according to Final Value Theorem. Parameters of the actual FF compensators are listed in Table 5.

Table 5. Parameters of two-mass model-based feedforward design

J_{mr}	3.64×10^{-4} kgm^2	J_{lr}	8.4×10^{-4} kgm^2
D_{mr}	21×10^{-4} Nms/rad	D_{lr}	12×10^{-4} Nms/rad
K_{gr}	2.48 Nm/rad	ω_c	$2\pi\times40$ rad/s

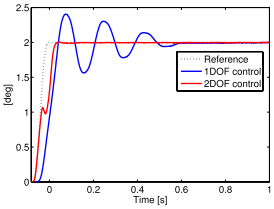

(a) 15 kg load

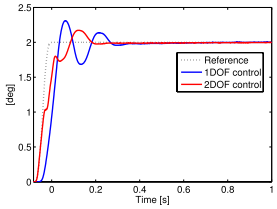

(b) 12.5 kg load

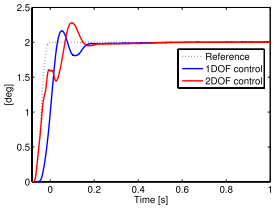

(c) 10 kg load

Fig. 8. Waveforms of arm position (θ_a) with conventional P-PI control systems

2.3 Vibration Suppression Performance of Conventional Control Systems with Load Variation Figure 8 shows comparative experimental response waveforms of arm position with conventional 1-DoF and 2-DoF control systems, for a typical short-stroke positioning with amplitude of 2 deg. As for the case of 15 kg, which the nominal model is constructed based on, the 2-DoF control shows an effective vibration suppression compared with the 1-DoF control. When the load weight decreases to 12.5 and 10 kg while FF compensators are kept unchanged, the motion performance with the 2-DoF control becomes worse.

To eliminate the effect of load variation in control performance, the parameters J_l and K_2 should be identified and updated inside FF compensators corresponding to the load changes. Nevertheless, it is not always possible to obtain their precise values because of nonlinearities and complexity of mechanical structure. Accordingly, a robust FB controller design is expected to ease the 2-DoF control performance deterioration following the model error.

3. H_∞ Synthesis-based Feedback Control Design

3.1 Gain-shaping Problem for 2-DoF Cascade Closed-loop Control System A common approach to achieve the robust performance of FB control system is H_∞ mixed-sensitivity synthesis [5]. It aims at shaping the gains of the closed-loop transfer function $S(s)$ from the output disturbance to the output, which is called *sensitivity function*, and the closed-loop transfer function $T(s)$ from the reference to the output, called *complementary sensitivity function*. For the cascade closed-loop control system, the sensitivity and complementary sensitivity functions are computed as follows:

$$S(s)=\frac{1+C_v(s)sP_m(s)}{1+C_v(s)sP_m(s)+C_p(s)C_v(s)P_a(s)},\quad\cdots\cdots(12)$$

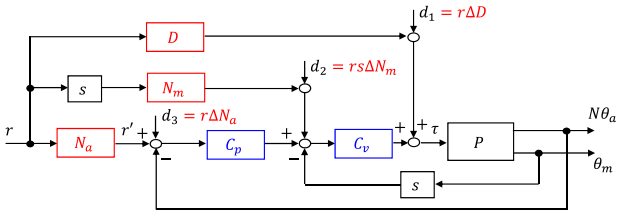

Fig. 9. Block diagram of 2-DoF control system with presence of model errors in FF compensators

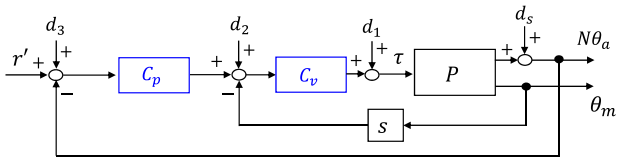

Fig. 10. Block diagram of FB control system with disturbances

$$T(s)=\frac{C_p(s)C_v(s)P_a(s)}{1+C_v(s)sP_m(s)+C_p(s)C_v(s)P_a(s)}.\cdots\cdots(13)$$

In the 2-DoF control system, not only two above sensitivity functions, but the effect of model errors in FF compensators is also considered. The influence of the difference between the ideal FF compensators that fits with actual plant, and the actual FF compensators that are calculated from the nominal model, is characterized by the disturbances d_1, d_2, and d_3 shown in Fig. 9. The closed-loop transfer functions from d_1, d_2, and d_3 to the output $N\theta_a$, denoted by $G_{d1}(s)$, $G_{d2}(s)$, and $G_{d3}(s)$, respectively, can be determined as follows:

$$G_{d1}(s)=\frac{P_a(s)}{1+C_v(s)sP_m(s)+C_p(s)C_v(s)P_a(s)},\quad\cdots\cdots(14)$$

$$G_{d2}(s)=\frac{C_v(s)P_a(s)}{1+C_v(s)sP_m(s)+C_p(s)C_v(s)P_a(s)},\quad\cdots\cdots(15)$$

$$G_{d3}(s)=\frac{C_p(s)C_v(s)P_a(s)}{1+C_v(s)sP_m(s)+C_p(s)C_v(s)P_a(s)}.\cdots\cdots(16)$$

From the viewpoint of FB control system shown in Fig. 10, the gains of transfer functions from all disturbances including the output disturbance d_s and FF-generated ones: d_1, d_2, and d_3, to the output should be bounded. The disturbance rejection requires adding the three transfer functions $G_{d1}(s)$, $G_{d2}(s)$, and $G_{d3}(s)$ to the gain-shaping problem, besides sensitivity function $S(s)$ and complementary sensitivity function $T(s)$. Notice that $G_{d3}(s)$ is identical to $T(s)$, thus, in total there are four transfer functions $S(s)$, $T(s)$, $G_{d1}(s)$, and $G_{d2}(s)$ included in the gain-shaping problem of H_∞ design.

3.2 Structure of H_∞ Synthesis Figure 11 shows a block diagram of the H_∞ synthesis proposed for the problem of shaping four transfer functions $S(s)$, $T(s)$, $G_{d1}(s)$, and $G_{d2}(s)$. The position and velocity controllers are combined into a controller $\mathbf{K}(s)$ whose two inputs are the trajectory tracking error $r'-N\theta_a$ and the motor velocity $\omega_m=\dot{\theta}_m$, with one output is the torque τ_{ref}, as follows:

$$\tau_{ref}=\mathbf{K}(s)\begin{bmatrix} r'-N\theta_a \\ \omega_m \end{bmatrix}\cdots\cdots(17)$$

$$=\begin{bmatrix} K_1(s) & -K_2(s) \end{bmatrix}\begin{bmatrix} r'-N\theta_a \\ \omega_m \end{bmatrix}.\cdots\cdots(18)$$

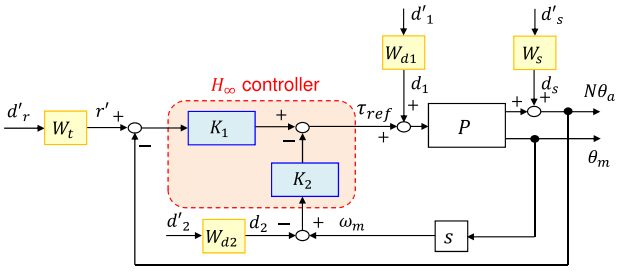

Fig. 11. Block diagram of H_∞ synthesis

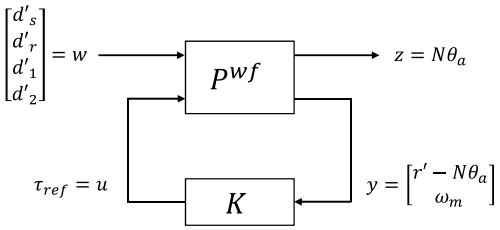

Fig. 12. Simplified diagram of H_∞ synthesis

Four weighting functions $W_s(s)$, $W_t(s)$, $W_{d1}(s)$ and $W_{d2}(s)$ are applied to output's disturbance d_s, reference r', FF-generated disturbances d_1 and d_2, respectively.

The system in Fig. 11 can be converted to the classical formulation of H_∞ synthesis as shown in Fig. 12, where the augmented plant P^{wf} is composed of the ordinary plant P and the weighting functions. Then, the generalized closed-loop function T_{zw} from the disturbance

$$w = \begin{bmatrix} d'_s & d'_r & d'_1 & d'_2 \end{bmatrix}^T \cdots\cdots (19)$$

to the evaluation output $z = N\theta_a$ is given by

$$T_{zw} = \begin{bmatrix} W_sS & W_tT & W_{d1}G_{d1} & W_{d2}G_{d2} \end{bmatrix}, \cdots\cdots (20)$$

where $S(s)$, $T(s)$, $G_{d1}(s)$, and $G_{d2}(s)$ are determined by

$$S(s) = \frac{1 + K_2(s)sP_m(s)}{1 + K_2(s)sP_m(s) + K_1(s)P_a(s)}, \cdots\cdots (21)$$

$$T(s) = \frac{K_1(s)P_a(s)}{1 + K_2(s)sP_m(s) + K_1(s)P_a(s)}, \cdots\cdots (22)$$

$$G_{d1}(s) = \frac{P_a(s)}{1 + K_2(s)sP_m(s) + K_1(s)P_a(s)}, \cdots\cdots (23)$$

$$G_{d2}(s) = \frac{K_2(s)P_a(s)}{1 + K_2(s)sP_m(s) + K_1(s)P_a(s)}. \cdots\cdots (24)$$

The task of design is to find the controller(s) $\mathbf{K}(s)$ that makes $\|T_{zw}(s)\|_\infty < 1$, then the gains of $S(s)$, $T(s)$, $G_{d1}(s)$, and $G_{d2}(s)$ are bounded by the inverse of corresponding weighting functions as follows:

$$|S(s)| < \left|\frac{1}{W_s(s)}\right|, \cdots\cdots (25)$$

$$|T(s)| < \left|\frac{1}{W_t(s)}\right|, \cdots\cdots (26)$$

$$|G_{d1}(s)| < \left|\frac{1}{W_{d1}(s)}\right|, \cdots\cdots (27)$$

$$|G_{d2}(s)| < \left|\frac{1}{W_{d2}(s)}\right|. \cdots\cdots (28)$$

3.3 Selection of Weighting Functions

Robustness of H_∞ synthesis-based control system greatly depends on the choice of weighting functions. Among the four weighting functions being considered, the two weights for the sensitivity and complementary sensitivity gains $|S(s)|$ and $|T(s)|$ should take priority because of their importance in robust stability of FB control system. The former specifies the tracking performance of FB system with the nominal plant, while the latter guarantees the robust stability against model error.

In detail, to obtain a nominally stable FB system, $|S(s)|$ should be kept small by choosing $|W_s(s)|^{-1}$ having a small upper-limit. Moreover, an ideal $W_s(s)$ should have an integral part s^{-1} to eliminate steady error. However, H_∞ control techniques generally requires that the weighting functions contains no unstable poles [17], hence an alternative integral part $(s + \epsilon)^{-1}$, where ϵ is a small positive number. The following function satisfying the above specifications has been selected for sensitivity function's weight:

$$W_s(s) = 0.32\frac{s + 2\pi \cdot 2}{s + 0.001}. \cdots\cdots (29)$$

As for the complementary sensitivity function's weight, $|W_t(s)|$ should be greater than the gain of multiplicative uncertainty for every frequency:

$$|\Delta W_t(s)| > |\Delta_m(s)| = \left|\frac{P(s) - P_n(s)}{P_n(s)}\right|, \cdots\cdots (30)$$

where $P(s)$ is the actual plant and $P_n(s)$ is the nominal model.

The nominal complementary sensitivity function then satisfies the following inequality:

$$|T(s)| < \left|\frac{1}{W_t(s)}\right| < \left|\frac{1}{\Delta_m(s)}\right|. \cdots\cdots (31)$$

Thus, according to the small gain theorem, the closed-loop is robustly stable with all designated cases of multiplicative uncertainty [18]. The weighting function that meets the condition (30) is chosen as follows:

$$W_t(s) = \left(90\frac{s + 2\pi \cdot 20}{s + 2\pi \cdot 2000}\right)^4 \cdot \frac{s^2 + 240.5s + 2988}{s^2 + 1.093s + 2988}. \cdots\cdots (32)$$

Figure 13 illustrates the satisfaction of the above weighting function with the requirement (30). The gain of $\Delta_m(s)$ always has a peak at the anti-resonant frequency of the nominal plant. Therefore, the Notch filter, which is the second factor in expression (32), has been applied to make $|W_t(s)|$ cover these peaks.

Finally, the weights for $|G_{d1}(s)|$ and $|G_{d2}(s)|$ are selected such that these gains do not exceed -14 dB, as follows:

$$W_{d1}(s) = 5\frac{s + 2\pi \cdot 0.5}{s + 0.0001}, \cdots\cdots (33)$$

$$W_{d2}(s) = 5. \cdots\cdots (34)$$

3.4 Calculation and Normalization of H_∞ Controller

An H_∞ controller including two stable 3^{rd}-order transfer functions $K_1(s)$ and $K_2(s)$ is obtained using non-smooth H_∞ synthesis [19], which is implemented by MATLAB *Robust Control Toolbox*'s function **Hinfstruct**. In order to make the proposed H_∞ controller work together with the FF compensators as well as make comparisons between controller designs become clearer, the two-input-one-output controller in

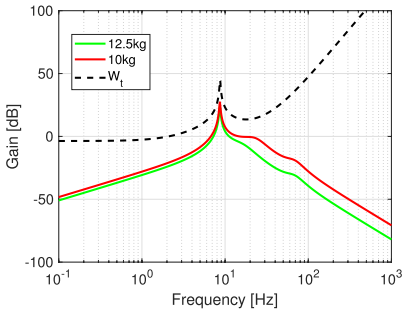

Fig. 13. Gain characteristics of multiplicative uncertainty $\Delta_m(s)$ in cases of 12.5 and 10 kg load, and weighting function $W_t(s)$

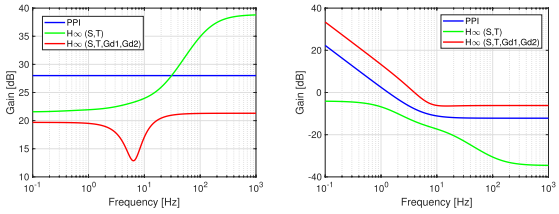

(a) (b)

Fig. 14. Gain characteristics of position controller $C_p(s)$ (a), and velocity controller $C_v(s)$ (b)

Fig. 11 is converted into position and velocity controllers the same as the conventional structure shown in Fig. 6, by the following formulations:

$$C_p(s) = \frac{K_1(s)}{K_2(s)}, \quad \cdots\cdots (35)$$

$$C_v(s) = K_2(s). \quad \cdots\cdots (36)$$

Figure 14 shows the gain characteristics of $C_p(s)$ and $C_v(s)$ with conventional P-PI (blue lines), traditional H_∞ mixed sensitivity synthesis-based (green lines), and the proposed H_∞ synthesis-based (red lines) designs. The traditional H_∞ synthesis without shaping $|G_{d1}(s)|$ and $|G_{d2}(s)|$ gives the velocity controller $C_v(s)$ with small gain at low frequency range, which potentially leads to steady-state errors. As for the proposed one, since equations (23), (24) and (36), we obtain:

$$C_v(s) = \frac{G_{d2}(s)}{G_{d1}(s)}. \quad \cdots\cdots (37)$$

Therefore, the desired shape of $|C_v(s)|$ can be achieved by shaping $|G_{d1}(s)|$ and $|G_{d2}(s)|$.

3.5 Robustness Improvement with H_∞ Controller

The evaluation of robustness with the proposed H_∞ control and the conventional P-PI control-based designs is firstly shown by frequency response shapes. Figure 15 shows the gain characteristics of four transfer functions $S(s)$, $T(s)$, $G_{d1}(s)$, and $G_{d2}(s)$, with the selected corresponding weighting functions. Comparing the two designs, a lower gain characteristic of the complementary sensitivity function $T(s)$ for every frequency is obtained with the H_∞ controller. As for the sensitivity function, the gain $|S(s)|$ is reduced at vibration frequency, however, increases at low-frequency range. It can be explained by the waterbed effect, or Bode's sensitivity integral [20]. In fact, a slight increase in $|S(s)|$ at low frequencies is acceptable because the tracking performance of 2-DoF control system is decided by FF compensators according to

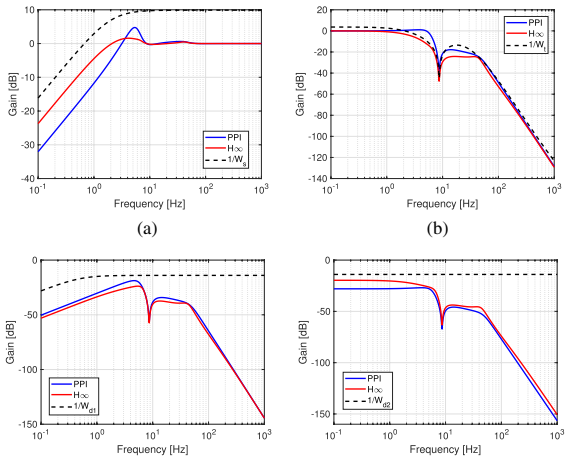

(a) (b) (c) (d)

Fig. 15. Gain characteristics of four transfer functions: (a) Sensitivity function $S(s)$, (b) Complementary sensitivity function $T(s)$, (c) d_1-disturbance rejection function $G_{d1}(s)$, (d) d_2-disturbance rejection function $G_{d2}(s)$

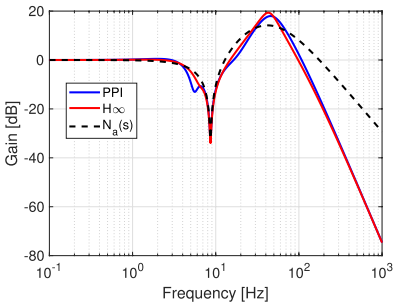

Fig. 16. Gain characteristics of tracking closed-loop function

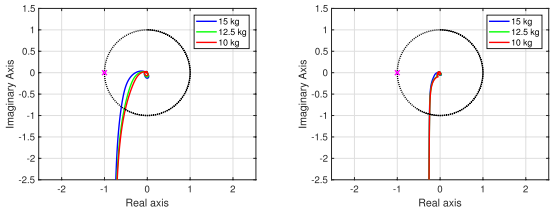

(a) (b)

Fig. 17. Nyquist plots: (a) P-PI control, (b) H_∞ control.

the equation (6). Figure 16 shows the tracking closed-loop characteristics $T_{yr}(s)$ for the nominal case, with the FF characteristic $N_a(s)$. It can be seen that the bandwidth of tracking closed-loop function is almost the same between two designs.

Furthermore, the robust stability is proven by the Nyquist plots of open-loop as shown in Fig. 17. The H_∞ control design (b) shows Nyquist loci further away from the point $(-1; 0)$ than those of the P-PI control design (a).

To clarify the improvement of robust performance, some numerical evaluations are listed in Table 6. By using H_∞ control, the gain and phase margins are improved noticeably, while the peak gains of sensitivity functions are also suppressed considerably.

4. Acceleration Feedback Control

The acceleration feedback (AFB) has been commonly used to improve the disturbance rejection performance in vibration

Table 6. Comparison of robustness criteria

	Conventional P-PI control	Proposed H_∞ control
Gain margin [dB]	11.26	23.59
Phase margin [deg]	52.75	75.60
$\|S\|_{\max}$ [dB]	4.74	1.58
$\|T\|_{\max}$ [dB]	1.05	0.001

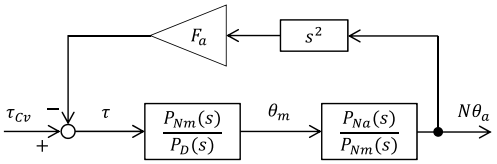

Fig. 18. Plant with acceleration feedback

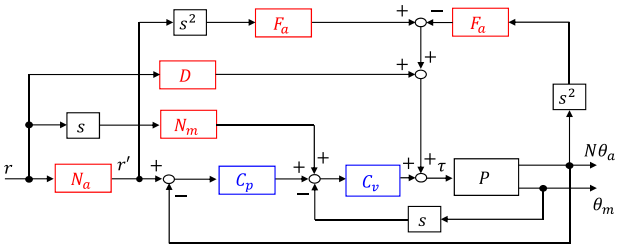

Fig. 19. Block diagram of 2-DoF cascade closed-loop control system with acceleration feedback

suppression control systems [11][12][21][22]. In this application, due to the lack of load accelerometer at the arm tip, only arm acceleration at the gearing's output is fed back to the motor torque. An observer of load acceleration at the arm tip will be considered for future works.

Figure 18 shows the block diagram of the new plant with acceleration feedback, where τ_{Cv} is the velocity controller output, and F_a is the AFB gain. The transfer functions of the new plant are then expressed as follows:

$$P'_m(s) = \frac{\theta_m(s)}{\tau_{Cv}(s)} = \frac{P_{Nm}(s)}{P_D(s) + F_a s^2 P_{Na}(s)} = \frac{P_{Nm}(s)}{P'_D(s)}, \quad \cdots\cdots (38)$$

$$P'_a(s) = \frac{N\theta_a(s)}{\tau_{Cv}(s)} = \frac{P_{Na}(s)}{P_D(s) + F_a s^2 P_{Na}(s)} = \frac{P_{Na}(s)}{P'_D(s)}. \quad \cdots\cdots (39)$$

Comparing the plants with and without AFB, the numerators keep constant while the denumerator increases by $\Delta P_D(s) = F_a s^2 P_{Na}(s)$. Therefore, if adding

$$\frac{\Delta P_D(s)}{F_c(s)} = \frac{F_a s^2 P_{Na}(s)}{F_c(s)} = F_a s^2 N_a(s) \cdots\cdots (40)$$

to $D(s)$ in equation (5), the tracking closed-loop function $T_{yr}(s)$ expressed by equation (6) does not change. It leads to the derivation of the FF component that compensates for the AFB component, as shown in Fig. 19.

This design conserves the reference tracking characteristic but affects the disturbance rejection by changing $S(s)$, $T(s)$, $G_{d1}(s)$, and $G_{d2}(s)$ whose expressions are shown in equations (12)–(15). The common denumerator of those transfer functions is a high-order polynomial with the coefficients depending on F_a. The AFB gain can then be determined through a pole placement design [11][12]. However, an arbitrary pole

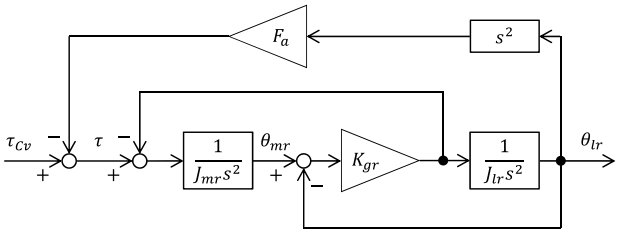

Fig. 20. Block diagram of undamped two-mass system with load acceleration feedback

Table 7. Acceleration feedback gain for load weights

Load weight	J_{mr}	J_{lr}	r_0	F_a
15 kg	3.64×10^{-4}	8.4×10^{-4}	1.82	5.6×10^{-4}
12.5 kg	3.64×10^{-4}	6.6×10^{-4}	1.68	7.4×10^{-4}
10 kg	3.64×10^{-4}	5.9×10^{-4}	1.62	8.1×10^{-4}

placement can not be performed here because the order of the denumerator is not less than 7 while the number of AFB parameters is only 1. Thus, the state feedback [23] should be applied together with the AFB design for a perfect theoretical approach.

For a simple theoretical calculation, we can obtain the AFB gain by using the following formula [21], under the assumption that the plant is an undamped two-mass system as shown in Fig. 20:

$$F_a = J_{mr}(r_d^2 - r_0^2), \cdots\cdots (41)$$

where r_d is the desired resonance ratio, and

$$r_0 = \sqrt{\frac{J_{mr} + J_{lr}}{J_{mr}}} \cdots\cdots (42)$$

is the natural resonance ratio without AFB ($F_a = 0$).

Briefly, the higher resonance ratio results in the better damping but the lower control bandwidth. The optimal range of resonance ratio, therefore, was given by Goubej [24] as $\sqrt{3} \le r \le \sqrt{5}$. In this stage, although the actual target system is a three-mass one, we theoretically apply this method under the assumption that the plant behaves like a two-mass system with the primary vibration mode. For a good damping performance, assign $r_d = 2.2$, then the calculation results of F_a corresponding to different load weights are listed in Table 7.

5. Experimental Results

The proposed controllers have been discretized using the bilinear transform with a sampling time of $T_s = 250\,\mu$s for experimentation. In all experiments, the robot arm is manipulated by the 2-DoF cascade closed-loop control framework with the consistent FF compensator design. An S-shaped position reference with 2-deg amplitude is applied the same as the experiments that are introduced in section 2.3.

Figure 21 shows comparative waveforms of arm position between different feedback controller designs, for different weights of load. The horizontal dashed lines denote the desired accuracy of ±0.02 deg, blue lines represent the conventional system based on P-PI control, while red lines represent the proposed system based on H_∞ control and acceleration feedback. The two more waveforms corresponding to P-PI controller with AFB (dotted cyan lines), and H_∞ controller

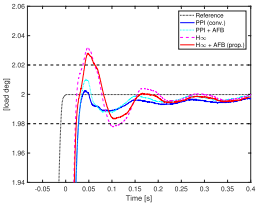

(a) 15 kg load

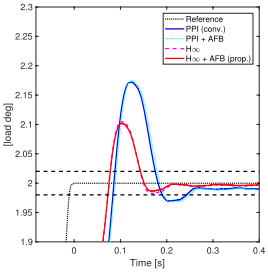

(b) 12.5 kg load

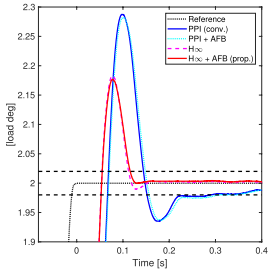

(c) 10 kg load

Fig. 21. Response waveforms of arm position (θ_a) with different controller types

without AFB (dashed magenta lines), are added in this comparison to clearly indicate the importance of each component in the combination of H_∞ controller and AFB.

The difference in response waveforms between controller designs is not considerable for the nominal case of 15 kg load because of insignificant model error. In the cases of 12.5 and 10 kg loads, the H_∞ control-based systems shows better performance with considerably smaller overshoot and faster response than the P-PI control-based ones. Between H_∞ synthesis-based systems, the design with AFB shows a slightly smaller overshoot and undershoot than the design without AFB.

6. Conclusion

In this paper, a 2-DoF cascade closed-loop control system consisting of static FF compensators and H_∞ synthesis-based robust FB controllers, combining with acceleration feedback, has been proposed to suppress the mechanical vibration due to the flexibilities of robot link and gearing for an actual single-axis robot arm. The static FF compensators have been computed based on co-prime factorization expression of an approximate two-mass model of the nominal plant for simplicity; while the FB controllers have been designed by a modification of H_∞ mixed-sensitivity synthesis considering disturbances from FF compensators. Acceleration feedback has been applied to the 2-DoF control system, aiming to increase the effectiveness of vibration suppression.

The robustness improvement of the proposed method has been proven by the drops in peak gains of sensitivity and complementary sensitivity functions as well as the increases in gain and phase margins. Also, the proposed design has been verified by experiments. In comparison with the conventional system using P-PI control, overshoot and settling time obtained by the proposed design remarkably decrease for the cases in which the model error becomes appreciable.

References

(1) M. Iwasaki: “Modeling and Compensation for Angular Transmission Errors for Precision Positioning Devices with Harmonic Drive Gearings”, Proc. of 6th International Conference on Positioning Technology, pp.13–20 (2014)

(2) L. Wang, S.G. Nurzaman, and F. Iida: “Soft-Material Robotics”, Foundations and Trends in Robotics, Vol.5, No.3, pp.191–259 (2014)

(3) K. Glover and D. McFarlane: “Robust stabilisation of normalised coprime factor plant descriptions with H_∞ bounded uncertainty”, IEEE Trans. on Automatic Control, Vol.34, No.8, pp.821–830 (1989)

(4) R.Y. Chiang: “Theory and Weighting Strategies of Mixed Sensitivity H_∞ Synthesis on a Class of Aerospace Applications”, IFAC Proc. Volumes, Vol.27, No.13, pp.279–284 (1994)

(5) S. Skogestad and I. Postlethwaite: “Multivariable Feedback Control: Analysis and Design, 2nd Edition”, John Wiley & Sons (2005)

(6) H.G. Sage, M.F. Mathelin, and E. Ostertag: “Robust control of robot manipulators: A survey”, International Journal of Control, Vol.72, No.16, pp.1498–1522 (1999)

(7) P. Axelsson, A. Helmersson, and M. Norrlof: “H_∞-Controller Design Methods Applied to One Joint of a Flexible Industrial Manipulator”, IFAC Proc. Volumes, Vol.47, No.3, pp.210–216 (2014)

(8) M. Makarov, et al.: “Modeling and preview H_∞ control design for motion control of elastic-joint robots with uncertainties”, IEEE Trans. on Industrial Electronics, Vol.63, No.10, pp.6429–6438 (2016)

(9) S. Jin, R. Kikuuwe, and M. Yamamoto: “Improving velocity feedback for position control by using a discrete-time sliding mode filtering with adaptive windowing”, Advanced Robotics, Vol.28, No.14, pp.943–953 (2014)

(10) G. Ellis and R.D. Lorenz: “Comparison of motion control loops for industrial applications”, Conference Record of the 1999 IEEE Industry Applications Conference., Vol.4, pp.2599–2605, USA (1999)

(11) G. Zhang: “Comparison of control schemes for two-inertia system”, Proc. of the IEEE 1999 International Conference on Power Electronics and Drive Systems, Vol.1, pp.573–578 (1999)

(12) M. Kino, et al.: “A Vibration Suppression Control of Flexible Manipulator by Estimated Reaction Torque and Multiple Acceleration Feedback”, IEEJ Trans. on Industry Applications, Vol.119, No.12, pp.1477–1484 (1999)

(13) K. Itoh, M. Iwasaki, and N. Matsui: “Optimal design of robust vibration suppression controller using genetic algorithms”, IEEE Trans. on Industrial Electronics, Vol.51, No.5, pp.947–953 (2004)

(14) E. Wernholt and S. Gunnarsson: “Nonlinear Identification of a Physically Parameterized Robot Model”, In preprints of the 14th IFAC Symposium on System Identification, pp.143–148, Australia (2006)

(15) M. Iwasaki, K. Seki, and Y. Maeda: “High-Precision Motion Control Techniques: A Promising Approach to Improving Motion Performance”, IEEE Industrial Electronics Magazine, Vol.6, No.1, pp.32–40 (2012)

(16) Y. Hori: “Vibration Suppression and Disturbance Rejection Control on Torsional Systems”, Proc. of IFAC Workshop on Motion Control, pp.41–50, Munchen (1995)

(17) K. Zhou: “Essentials of Robust Control”, Prentice Hall (1999)

(18) W.S. Levine: “The Control Handbook”, sec. 31.2.5: Robust Stability, pp.539–540, CRC Press (1996)

(19) P. Apkarian and D. Noll: “Nonsmooth H-infinity Synthesis”, IEEE Trans. on Automatic Control, Vol.51, No.1, pp.71–86 (2006)

(20) H.W. Bode: “Network Analysis and Feedback Amplifier Design”, D. van Nostrand, New York (1945)

(21) V. Helma, M. Goubej, and O. Jezek: “Acceleration Feedback in PID Controlled Elastic Drive Systems”, IFAC-PapersOnLine, Vol.51, No.4, pp.214–219 (2018)

(22) K. Ito and M. Iwasaki: “State Feedback-based Vibration Suppression for Multi-axis Industrial Robot with Posture Change”, 42nd Annual Conference of the IEEE Industrial Electronics Society, IECON 2016 (2016)

(23) Y. Hori, H. Iseki, and K. Sugiura: “Basic Consideration of Vibration Suppression and Disturbance Rejection Control of Multi-Inertia System using SFLAC (State Feedback and Load Acceleration Control)”, IEEE Trans. on Industrial Applications, Vol.30, No.4, pp.889–896 (1994)

(24) M. Goubej: “Fundamental performance limitations in PID controlled elastic two-mass systems”, IEEE International Conference on Advanced Intelligent Mechatronics (AIM) (2016)

Tran Vu Trung (Student Member) received the B.E. degree in Control and Automation Engineering from Hanoi University of Science and Technology, Vietnam, in 2015. Currently, he is a Master degree student of Department of Electrical & Mechanical Engineering, Nagoya Institute of Technology, Japan. His current research interests are motion control of mechatronic and robotic systems. Mr. Tran is a student member of IEEE.

Makoto Iwasaki (Senior Member) received the B.S., M.S., and Dr.Eng. degrees in electrical engineering and computer science from Nagoya Institute of Technology, Japan, in 1986, 1988, and 1991, respectively. Since 1991, he has been with the Department of Computer Science and Engineering, Nagoya Institute of Technology, where he is currently a Professor. His current research interests are applications of control theory and soft computing techniques for motor/motion control. Dr. Iwasaki is a fellow of IEEE.